Eur. Phys. J. B **46**, 1–8 (2005)
DOI: 10.1140/epjb/e2005-00232-2

THE EUROPEAN PHYSICAL JOURNAL B

Position control and optical manipulation for nanotechnology applications

M. Capitanio[1], R. Cicchi[2], and F.S. Pavone[2,a]

[1] LENS, Via Nello Carrara 1, 50019 Sesto Fiorentino, Firenze, Italy and Dipartimento di Biologia Animale e Genetica "Leo Pardi", Via Romana 17/19 50125 Firenze, Italy
[2] LENS, Via Nello Carrara 1, 50019 Sesto Fiorentino, Firenze, Italy and Dipartimento di Fisica-Università degli Studi di Firenze, Via Giovanni Sansone 1, 50019 Sesto Fiorentino, Firenze, Italy

Received 8 September 2004 / Received in final form 6 April 2005
Published online 8 August 2005 –

Abstract. During the last decade, great advances have been made concerning the construction and manipulation of nanostructures. As a consequence, nanometer stability and control of the sample position have became crucial points. For this purpose, we have built an optical microscope with high mechanic stability and we have implemented a feedback system in order to compensate thermal drifts. We demonstrate the system stability to be within one nanometer, with a control on the sample position of some micrometers, along the three spatial directions. The sample can be manipulated optically by means of a multiple optical tweezers setup and its displacements measured with a 3D position detector. We discuss and characterize the system properties thoroughly. We finally test the apparatus on a bio-molecular system constituted by a single myosin motor interacting with an actin filament.

PACS. 07.05.Dz Control systems – 87.80.Cc Optical trapping – 82.37.Rs Single molecule manipulation of proteins and other biological molecules

1 Introduction

Visualization and manipulation of particles with dimensions on the nanometer scale rely on recently developed techniques, mainly scanning probe microscopes [1] and advanced optical microscopes and tweezers [2]. Although conventional optical and fluorescence microscopy are limited by light diffraction, which for visible light is about $\lambda/2 \simeq 250$ nm [3], in recent years a lot of techniques have overcome the diffraction limit. Among these, particle localization and tracking techniques can achieve a precision greater by one or two orders of magnitude with respect to the resolution of a conventional optical microscope [4], reaching the nanometer resolution. The high precision of these techniques allowed single biomolecule studies such as the molecular motions on living cell surfaces [5], individual protein in solution [6] and in cells [7], and the interaction of Lac-repressor with a single DNA molecule [8]. Moreover, new concepts in microscopy have emerged that have overcome the diffraction barrier. Its first exponent is the stimulated emission depletion microscopy, which has so far displayed a resolution down to 28 nm [9]. Furthermore, the integration of optical tweezers within conventional microscopes has allowed manipulating particles with dimensions ranging from some nanometers to some microns and measuring forces and displacements respectively from fractions of piconewton to hundreds of piconewton and from fractions of nanometer to hundreds of nanometers [2]. Due to the range of forces and displacements exerted, optical tweezers have been largely used in single bio-molecules experiments [10]. Other applications have included fabrication and shaping of nano and micro structures through optical scalpels and scissors [11,12] or spatially resolved photochemistry [13] and their precise positioning and fixation [14–16]. All these new techniques have brought the need of nanometer stabilization and position control of optical microscopes and optical tweezers. The approaches used so far to solve this question have been both to build structures with high stability or to modify commercial optical microscopes, in order to obtain an increased mechanical stability. In any case, the apparatus must be isolated as well as possible from external mechanic, acoustic and thermal noise. In reference [17], the microscope body was extensively modified and situated on an optical air table, inside a temperature-controlled, sound-proofed clean room, reducing the drift of the system to 0.5 nm/min. The disadvantage of such an approach is that the operation of the system has to be performed with remote control outside the room that contains the microscope. Recently, a new approach to the problem has been adopted in order to study the binding sites of myosin molecules on actin

[a] e-mail: pavone@lens.unifi.it

filaments [18]; in that experiment, a commercial microscope has been used together with a feedback system capable of compensating thermal drifts by servo-controlling the position of a 1.5 μm diameter bead fixed to the microscope slide, obtaining an RMS noise of about one nanometer along the x and y axes, and of 5 nm along the z axis.

Here, we have built a custom mechanical structure with increased mechanical stability and we have integrated the custom microscope with a feedback system capable of compensating thermal drifts. The working principle of the feedback system is simple and similar to that reported in reference [18], but with two major changes: 1) a filter is applied to the bead image, which together with the high mechanic stability of the microscope, reduces the RMS noise of the system below 1 nm along the three spatial directions; 2) the system is capable of controlling the sample position for a range of some micrometers, while still maintaining sub-nanometer stability.

In this paper, the main effort is devoted to give a complete characterization of the system, to describe the methods and techniques used to compensate thermal drifts and to reduce the noise components of the apparatus. The method used to derive the position of the fixed bead along the three spatial directions is described along with the feedback system and the position control procedure. The feedback system has been calibrated and characterized and the noise components throughly analyzed. We have finally tested the apparatus on a bio-molecular system constituted by a single myosin motor interacting with an actin filament, demonstrating both the stability and the position control capabilities of the system.

2 The experimental apparatus

The experimental apparatus was built around a custom made mechanical structure. A custom structure was used to obtain high mechanical stability and to make use of optics specifically designed for the optical tweezers (infrared laser). The mechanical structure is made of ERGAL (Erbium, Gallium, Aluminium) and is composed by three 250 × 250 × 30 mm platforms held by four stainless steel columns 25 mm diameter, 500 mm high (see Fig. 1). The optical axis of the microscope coincides with the center of the platforms; for this reason, the center of the platforms has been bored to allow the passage of the light. The lower platform serves as a basis for the whole microscope. On the middle platform, two manual translators (M-014 Physik Instrumente) allow gross movements of the sample in the xy plane (25 mm of excursion in each direction), while a piezoelectric translator (P-527.2CL Physik Instrumente), mechanically coupled to the manual ones by means of a horizontal ERGAL platform, allows fine movements (200 μm of excursion, 1 nm minimum displacement). The objective (Nikon Plan-Apo 60X, N.A. 1.20, W.D. 0.2 mm, water immersion) is positioned along the optical axis by means of two orthogonal ERGAL brackets fixed at the middle platform and sits over a piezoelectric translator for z movements (P-721.20 Physik Instrumente, 100 μm of excursion, 1 nm minimum displacement). The higher platform serves as a basis for the detection system and the support structure of the condenser. The condenser (Olympus U-AAC, Aplanat, Achromat, 1.4 NA, oil immersion) is mounted on a support which can be translated vertically to lift it when the sample needs to be positioned or removed (Fig. 1 shows the configuration with the condenser in the upper position). By adjusting five screws, the condenser can also be finely translated along the z direction in order to be properly focused and along the xy plane in order to be properly centered along the optical axis. A schematic drawing of the experimental apparatus is depicted in Figure 2. The optical microscope is supplied with a CCD for wide field magnification (CCD 200X, Hamamatsu C3077), a CCD for high magnification (CCD 2000X, Ganz ZC-F11C3) and an intensified CCD (Hamamatsu C2400) for fluorescence microscopy. The image coming from the high magnification camera is acquired by a digitalizing board mounted on the PC, and is used by the feedback system (as explained in Sect. 4). A halogen lamp (Schott KL1500LCD, 150 W) supplies illumination for bright field microscopy, while a laser beam coming from a Nd:YAG duplicated laser, emitting at 532 nm (VERDI, Coherent, Verdi V-10), supplies illumination for fluorescence microscopy. A double optical tweezers setup is integrated within the microscope; this is obtained by splitting the beam coming from a Nd:YAG laser (Spectra-Physics Millennia IR, $\lambda = 1064$ nm) into two beams with orthogonal polarizations. A double acousto-optic modulator (AOM, A&A DTS-XY 250) placed in the path of one of the two beams provides fine movements of one trap within the sample (0.1 nm minimum displacement), while a quadrant detector photodiode (QDP, UDT DLS-20) placed in the back focal plane of the condenser provides 3D position detection of the bead with nanometer resolution [19]. The detection of one of the two traps is selected by rotating a polarizer positioned in front of the quadrant detector photodiode.

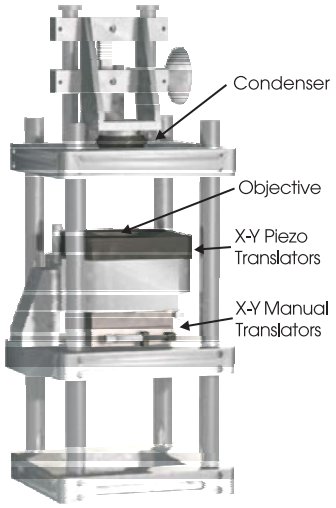

Fig. 1. The mechanical structure that constitutes the optical microscope.

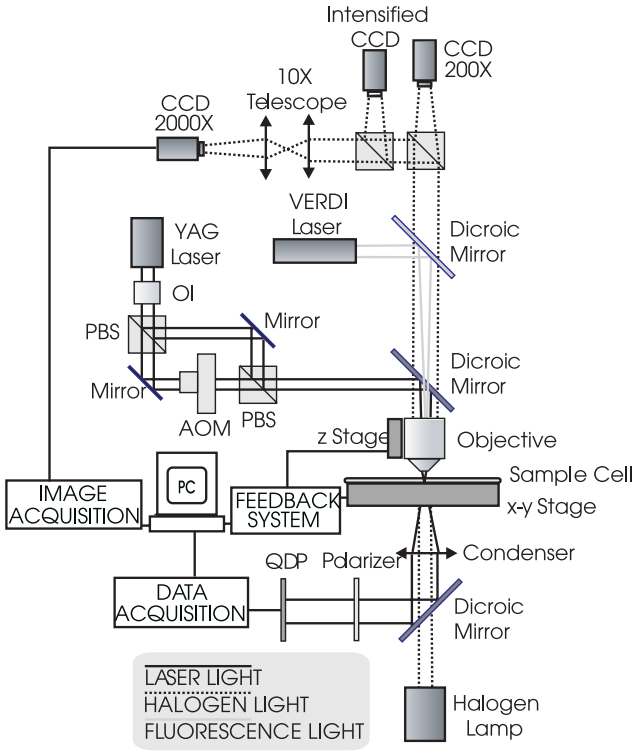

Fig. 2. A schematic drawing of the experimental setup. OI: Optical isolator, PBS: polarizing beam-splitter cube, AOM: acousto-optic modulators, QDP: quadrant detector photodiode.

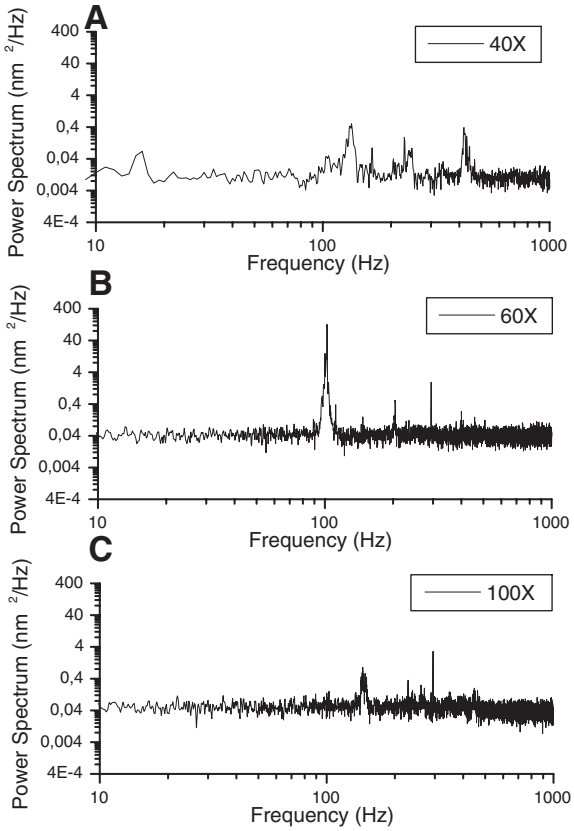

Fig. 3. The power spectra of the stage position along the z axis, obtained with three different objectives. Each spectrum is a mean of 100 spectra obtained from 1 second of acquisition. A) 40X objective (medium weight). B) 60X objective (the heaviest). C) 100X objective (the lightest). The lower peak frequency decrease with increasing load on the piezoelectric stage.

3 Limiting sources of noise

At the nanometer level, the image produced by the microscope and the laser trap are affected by various sources of noise. Acoustic noise usually affects frequencies ranging from about 10 Hz to some KHz, while mechanical noise and thermal drifts usually affect lower frequencies. Acoustic noise may also be enhanced by resonances of the microscope mechanical structure or of the optics mountings. We limited mechanical vibrations by mounting the experimental setup on an optical table equipped with active isolators (Melles-Griot). The microscope structure was mounted over three rubber pedestals with honeycomb structure, which absorbed a fraction of the mechanical oscillations in the acoustic range of frequencies. In order to avoid additional mechanical and acoustic noise, we put acoustically loud devices, in particular those equipped with cooling fans, outside of the table and we enclosed the apparatus in a chamber of plastic panels; the panels can slide in order to make the apparatus accessible during operation and to be completely closed during measurements. The piezoelectric translators are equipped with a capacitive position detector with sub-nanometer resolution and with electronics (Physik Instrumente E-516.13) providing a feedback loop that stabilizes the stages position from piezoelectric hysteresis and thermal drifts. Nevertheless, the translators feedback does not compensate drifts of the stages relative to the objective or thermal expansions of the optics, which change the microscope image and the trap position relative to the sample. Such thermal drifts are compensated by our feedback system, as explained in Section 4. We found that the sustain of the objective was the main source of mechanical noise in the acoustic range of frequencies (100 Hz–1 kHz). This fact is evidenced by the power spectra of the position signal coming from the piezoelectric capacitive sensor. Figure 3 shows the spectra obtained with 40X, 100X and 60X objectives mounted on the z translator. At least one peak within the noise spectra at a frequency which varies with the mounted objective is clearly visible in the figure; the lower peak frequency decreases with the increasing weight of the objective. The sustain of the objective was initially constituted by an ERGAL bracket fixed on the middle platform and a mobile bracket connected to a vertical manual translator (Physik Instrumente 8290). In order to reduce the mechanical noise, we have directly fixed the sustain of the objective on the middle platform. Figure 4 shows the power spectra after removal of the z manual translator, evidencing a clear decrease in the noise peaks.

The laser trap is also affected by other sources of noise. We have found the pointing stability of the laser beam sensibly depending on the air turbulence, and we enhanced it

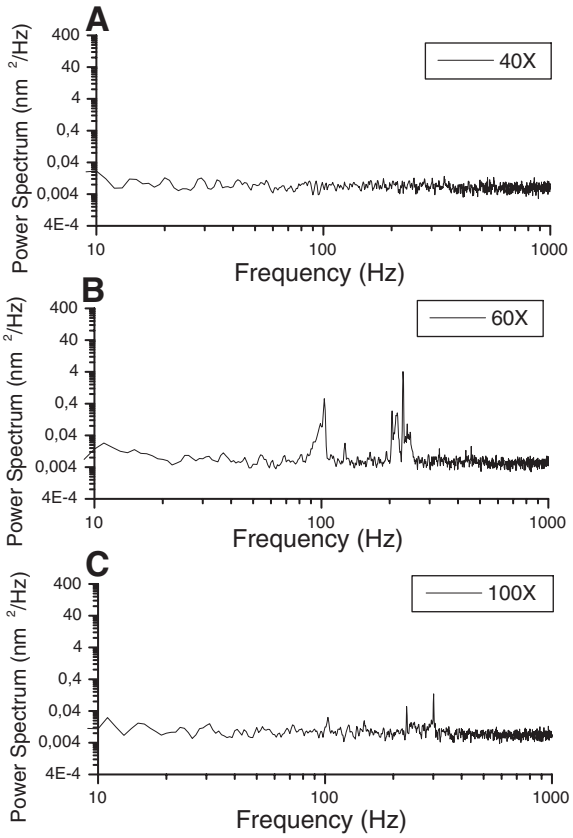

Fig. 4. The power spectra of the stage position signal along the z axis, obtained as in Figure 3, after removal of the z manual translator. A) 40X objective. B) 60X objective. C) 100X objective. The noise peaks are clearly reduced with respect to the spectra shown in Figure 3.

by enclosing the laser beam path into plastic tubes. Optical feedback, due to back-reflections of the beam inside the laser cavity, causes random amplitude fluctuations in the laser source. We limited it by placing an optical isolator in the laser path near the laser source.

4 Compensating thermal drifts

Even if the system has been proved to be mechanically stable, at the nanometer level thermal drifts in the optics and in the mechanical components of the microscope may change the image of the sample with time. This could be a serious problem both for high-resolution microscopy and for optical tweezers applications. In fact, if the sample image drifts with time, the trap position relative to the sample drifts too. In order to probe and correct thermal drifts, we implemented a feedback system based on a very high-magnification image of a silica bead (1.54 μm diameter, Bangslabs SS04N/5303) fixed on the coverslide. Coverslides covered with silica beads were obtained by spreading 1 μl of beads suspended in a solution of amyl acetate containing 1% nitrocellulose on the coverslide surface. The working principle of the feedback system is conceptually simple: the image from the high magnification

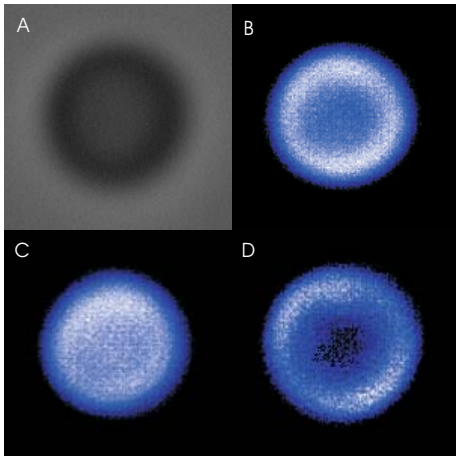

Fig. 5. Image of a 1.54 μm silica bead projected on the high magnification camera (A) and the same image after inversion and application of the threshold filter with $b = 90$ and $z = 0$ (B), $z = +250$ nm (C) and $z = -250$ nm (D).

camera (2000X) is first acquired by the digitalizing board on the PC. Then, the bead position along the x, y and z directions is calculated and, if the position changes with time, the piezoelectric translators are driven in order to correct the displacement.

4.1 The 3D centroid algorithm

The field of view of the high magnification camera is about 7×5 μm wide, acquired at 768×576 pixels, so that the bead image has a diameter of about 190 pixel. The operator can select a squared region that contains the bead image and the region image is digitalized at 8 bit of resolution. The region image is thus stored into a square matrix $M_{i,j}$ whose values range from 0 (black) to 255 (white). When the focal plane of the objective is positioned slightly above the bead, the bead image appears as a circle darker than the background, with a darker external ring (see Fig. 5A). The digitalized image of the region that contains the bead is first inverted and processed by a threshold filter in order to cut off all the background noise outside the bead:

$$I_{ij} = \frac{(b - M_{ij}) + |b - M_{ij}|}{2}, \qquad (1)$$

where I_{ij} is the inverted and processed image and b is a constant threshold value ranging from 0 to 255. When $b = 0$, $I_{ij} \equiv 0$ and the threshold filter cuts the whole image which appears fully black. When $b = 255$, $I_{ij} \equiv 255\text{-}M_{ij}$ and the image is simply inverted without any filtering. The b value is set to a value such that the background surrounding the bead results completely black, while the bead is still clearly distinguishable (see Fig. 5B). The X and Y position of the bead center is then obtained from the image centroid:

$$X = \frac{\sum_{ij} iI_{ij}}{\sum_{ij} I_{ij}} \quad ; \quad Y = \frac{\sum_{ij} jI_{ij}}{\sum_{ij} I_{ij}}. \qquad (2)$$

When the bead moves along the Z direction, the diffraction rings of the bead image change shape (see Fig. 5 B, C and D). The ratio between the total intensity of the pixels located in a region inside the bead and the total intensity of the pixels located outside that region will be shown to linearly depend on Z (see Sect. 4.2). The bead Z position is thus obtained from the ratio between the total intensity of a 25×25 pixels square centered inside the bead and the total intensity of the pixels outside that square:

$$Z = \frac{\sum_{|i-X|<25;|j-Y|<25} I_{ij}}{\left(\sum_{ij} I_{ij} - \sum_{|i-X|<25;|j-Y|<25} I_{ij}\right)}. \qquad (3)$$

While X and Y are expressed in pixels, Z is adimensional. In order to obtain from the bead position X, Y, and Z the real displacements in nanometers, the feedback system needs to be calibrated, as explained in the next section. Through the paper we indicate with x, y and z the displacements of the sample (expressed in nanometers) imposed by the piezo translators, whereas with X, Y and Z the displacements of the sample detected from the bead image through equations (2) and (3), expressed either in pixels for X and Y and adimensionally for Z, or in nanometers.

4.2 Calibration of the feedback system

In order to calibrate the feedback system, i.e. in order to obtain the nm/pixel conversion factors k_X, k_Y, and the nm conversion factor k_Z, the piezoelectric translators were moved along the x, y and z directions by 1 nm steps, while X, Y and Z were measured at every step. The stage stroke has to be fast enough to prevent thermal drifts from changing the bead position (Sect. 4.3). The X and Y bead positions (calculated from Eq. (2)) behave linearly respectively with the x and y bead displacements, in the whole range of positions where the bead image remains inside the acquired region (see Fig. 6A and 6B). The Z value (calculated from Eq. (3)) behaves linearly with the z bead displacement in a range of about ± 700 nm from the center of the bead (see Fig. 6C). From the inverse of the slopes of the curves depicted in Figure 6A, B and C, the conversion factors k_X, k_Y, and k_Z for the three directions were obtained. With our setup we evaluated $k_X = 9.757 \pm 0.005$ nm/pixel, $k_Y = 10.012 \pm 0.007$ nm/pixel, and $k_Z = (227.3 \pm 0.2) \times 10^3$ nm (errors from linear regression of data displayed in Fig. 6). While a translator was moved along the x (y, z) direction, the Y and Z (X and Z, X and Y) displacements were also recorded, in order to estimate the correlation between movements along one direction and detected movements along the other two directions. When the stage was moved along the x axis, the Y position translated proportionally, with a –0.04 slope (see Fig. 7A). This correlation is probably due to the presence of a non-zero angle α between the x axis of the piezoelectric translator and the X axis of the CCD camera. This is confirmed by the fact that when the stage was moved along the y direction, the X position translated proportionally with a +0.05 slope, that is consistent with an angle α=40–50 mrad (see Fig. 7B). Also Z showed a correlation with x and y displacements of the order of 1% (see Fig. 7A and Fig. 7B), which can be again explained by the presence of an angle of about 10 mrad between the z translator axis and the microscope optical axis. The

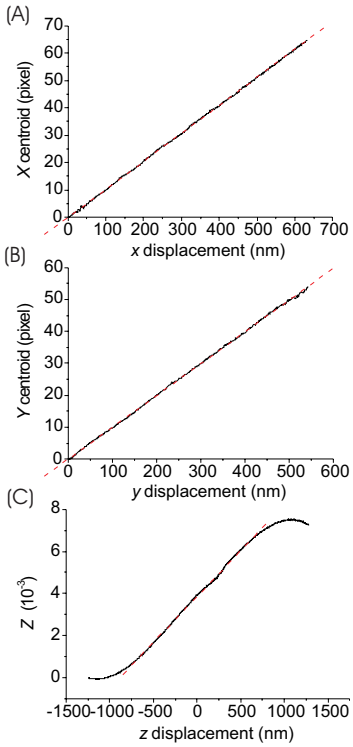

Fig. 6. Calibration curves for the x (A), y (B) and z (C) directions. Calibration curves have been obtained while moving the piezo translators at a constant speed of 25 nm/s.

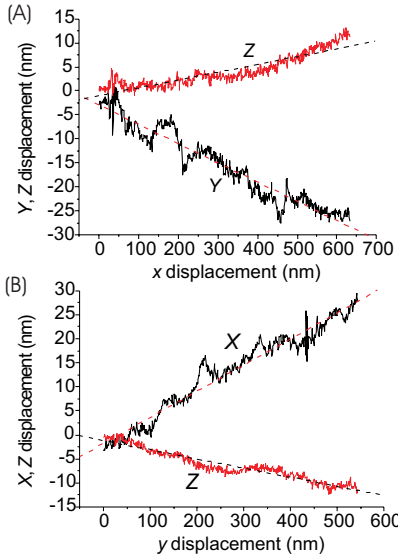

Fig. 7. (A) Correlation between x stage movements and Y and Z position detection. (B) Correlation between y stage movements and X and Z position detection. Both curves have been obtained while moving the piezo translators at constant speed of 25 nm/s.

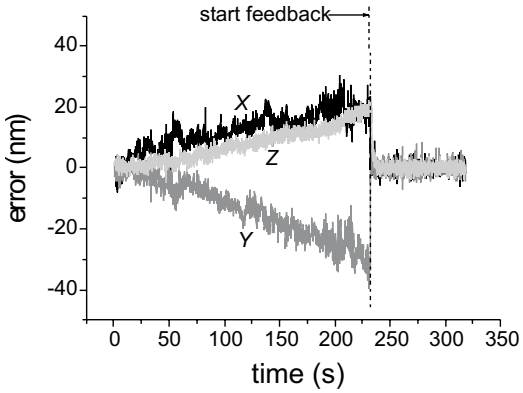

Fig. 8. The bead position error as a function of time. For time less than 230 s the feedback system is off, for time greater than 230 s the feedback is on ($g_x = g_y = g_z = 0.2$).

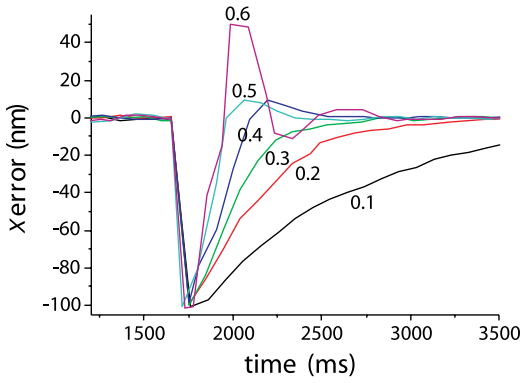

Fig. 9. Time response of the x feedback error after a 100 nm step displacement, for different gain values (0.1–0.6). Curves with $0.1 < g_X < 0.3$ are fitted by an exponentially decaying function; curves with $0.4 < g_X < 0.6$ are fitted by a sine function with an exponential envelope.

X and Y positions also showed some correlation with z displacements critically depending on the alignment of the optics placed along the illumination path. An accurate alignment is required in order to avoid such an effect.

4.3 Thermal drifts and the feedback system

When started, the feedback system calculates the initial coordinates of the bead X_0, Y_0, and Z_0. The software thus enters into a loop where the bead image is acquired, the bead position X, Y and Z is calculated, and the position error $e_X = X - X_0$, $e_Y = Y - Y_0$, and $e_Z = Z - Z_0$ is derived. The execution velocity of the loop is limited by the video acquisition rate (25 Hz). The software thus drives the piezoelectric translators in order to correct the error. The corrections c_X, c_Y, and c_Z (in nm) along the three axis are

$$c_X = -e_X k_X g_X; \tag{4}$$

$$c_Y = -e_Y k_Y g_Y; \tag{5}$$

$$c_Z = -e_Z k_Z g_Z, \tag{6}$$

where g_X, g_Y, and g_Z are the gains along the three directions. When $g_X = g_Y = g_Z = 0$, no correction is imposed by the feedback system and the bead position shows slow (usually about 10 nm in 100 s) random fluctuations due to thermal drifts (see Fig. 8). If $g_X = g_Y = g_Z = 1$, the feedback system corrects exactly by the same amount of the error. If the gain is set at a too high value, the system oscillates at the natural frequency of the system, whereas if the gain is too low, the correction is insufficient to correct thermal drifts. We have found the optimal gain to obtain maximum correction and to avoid auto-oscillations (see below) to range between 0.2 and 0.6 with our setup, depending on the halogen light intensity and the image acquisition board settings. With an optimal gain setting we obtained a RMS noise on the bead position of

$$\sigma_x = 0.89 \text{ nm}; \tag{7}$$

$$\sigma_y = 0.79 \text{ nm}; \tag{8}$$

$$\sigma_z = 0.81 \text{ nm}. \tag{9}$$

When the feedback system is up and running, the sample position can still be changed by changing the initial coordinates of the bead X_0, Y_0 and Z_0. The software is thus provided with three sliders in order to vary the x, y and z position of the sample by varying the initial coordinates as $X_0' = X_0 + x/k_X$, $Y_0' = Y_0 + y/k_Y$, $Z_0' = Z_0 + z/k_Z$. The time response of the feedback system depends on the gain settings. Figure 9 shows the time response of the X error after a 100 nm step of the initial position X_0, for different gain g_X values. Similar curves are obtained also along the y and z directions. The response is typical of a second order system [20], with a natural oscillation frequency and a damping factor which depends on the gain value. For low gain values (0.1–0.3 in Fig. 9), the system behaves as overdamped, whereas for high gain values (0.4–0.6 in Fig. 9), the system behaves as underdamped. The optimal gain setting corresponds to the critically damped motion, where no oscillations occur while the system maintains a fast temporal response (0.3–0.4 in Fig. 9).

The feedback system can be represented as a closed-loop system with negative feedback. It can be modeled as a proportional control with a Coulomb friction, independent of speed but acting in a direction to oppose motion [20]. The Coulomb friction is present because the stages cannot produce displacements smaller than 1 nm. $e_i^0 = 1 \text{ nm}/k_i g_i$ ($i = X, Y, Z$) is the amount of error that must exist before the piezoelectric translators can develop sufficient movement to overcome the "frictional force" and cause the stages to move. The presence of such Coulomb friction assure that once the gain is set at a small enough value (so that e_i^0 is big enough), the oscillations of the system are damped out. The advantage of such a system relies in its simplicity; it does not require any additional output

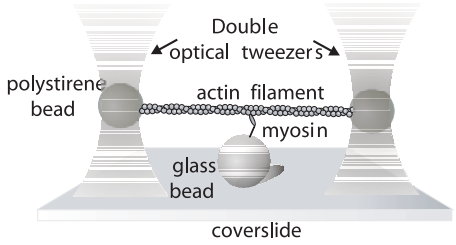

Fig. 10. The "three beads assay". The experimental assay used to study the interactions between a single myosin molecule (subfragment-1 extracted from mouse) and an actin filament.

velocity feedback damping in order to damp out oscillations. On the other hand, the Coulomb friction produces a dead-zone of width $2e_0$ about the equilibrium position, which means that if the system is initially in equilibrium it will not respond at all to variations unless $e > e_0$.

5 Test on a nanoscopic system

We have tested the apparatus on a single bio-molecule assay constituted by a myosin molecule interacting with an actin filament. Myosin is a motor protein almost ubiquitous in eukaryotic cells and responsible for many cellular motility processes. In particular, skeletal muscle myosin is the motor protein which drives muscle contraction. At the molecular level, force and movement are produced through cyclic interactions between myosin and actin coupled to the hydrolysis of ATP. In this process the chemical energy contained in the ATP molecule is converted into mechanical energy [21]. In the experimental assay, a single actin filament is suspended between two polystyrene beads (1.1 μm diameter) and presented to a myosin molecule bound to a glass bead (1.54 μm diameter) attached to a microscope coverslide [22] (see Fig. 10). The double optical tweezers hold the two polystyrene beads. Attachment between the beads and the actin filament is achieved using neutra-avidinated beads and biotinilated actin. The actin filament can be finely (sub-nanometer control) stretched by moving one of the two traps through the acousto-optic modulators. The glass bead is used as reference for the feedback system in order to maintain the position between actin and myosin within one nanometer. In order to monitor the position of the actin filament, we recorded the position of one of the two polystyrene beads using the QDP. When there are no interactions between actin and myosin, the bead position signal is that of a overdamped harmonic oscillator (due to the presence of the optical trap and the viscous solution) in a thermal bath (due to collisions with the molecules of the solution in which the bead is immersed). When the myosin molecule binds to actin, a noise reduction is clearly visible in the signal because of the higher stiffness of the molecule (of the order of 1 pN/nm) with respect to the optical tweezers (about 0.05 pN/nm, see Fig. 11). "Bound" and "unbound" states are, therefore, distinguished based on signal variance [23].

The myosin binding probability along the actin filament depends on the relative position of the two

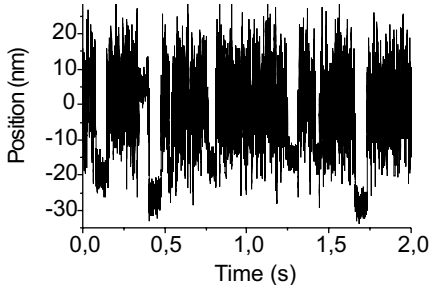

Fig. 11. Acto-myosin interactions. The figure shows two seconds of the position signal of one of the two polystyrene beads represented in Figure 10, while the myosin molecule is interacting with actin. When the myosin molecule binds to actin, a noise reduction is clearly visible in the signal.

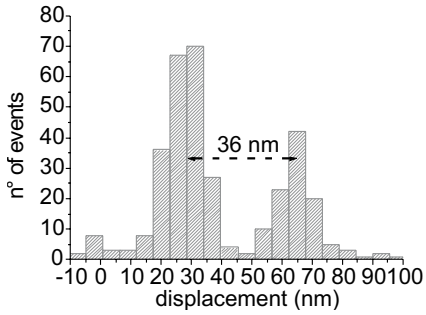

Fig. 12. Distribution of bound event sampled at 5 nm steps.

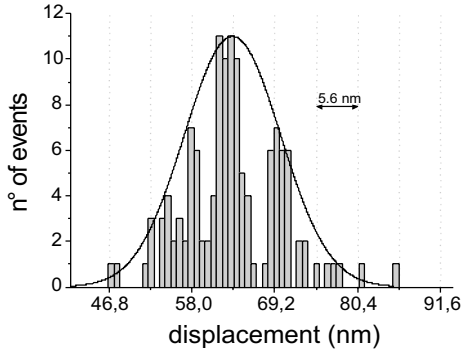

Fig. 13. Distribution of bound event sampled at 0.5 nm steps.

molecules. In fact, actin is a double helix polymer with a periodicity of 72 nm; myosin binds specifically to each actin monomer with a rate that depends on the orientation of the monomer along the filament [18]. We recorded 100 s of acto-myosin interactions while the myosin molecule was displaced 72 nm along the filament axis at constant velocity, using the position control capabilities of the feedback system. In this way, we were able to map the binding distribution along the filament axis (Fig. 12 and Fig. 13). The distribution of bound events sampled at 5 nm steps shows that the myosin molecule preferably binds on target zones spaced about 36 nm (half of the actin periodicity). The distribution of bound events within each target zone, sampled at 0.5 nm steps, shows that the myosin molecule binds to specific sites spaced $\sim$5.6 nm, in correspondence with the actin monomers disposed along the filament. Such results are in agreement with those reported

by Steffen et al. [18] and demonstrate the system stability and the capabilities of position control. Residual noise, particularly visible in the 0.5 nm distribution, is mainly due to the rotational Brownian noise of the actin filament, which randomizes the monomer orientation presented to the myosin molecule.

6 Conclusions

In conclusion, we have built an optical microscope with high mechanic stability over the acoustic range of frequencies and we have developed a feedback system which limits thermal drifts in the low range of noise frequencies.

We have first analyzed acoustic and mechanic sources of noise and we have given some prescriptions in order to reduce such contributions.

Thermal drifts in the system have been monitored by looking at the position of a bead fixed on the sample surface obtained from a 3D centroid algorithm, which has been described.

We have developed a calibration procedure to relate the position of the bead image with the displacement of the sample.

Finally, we have described and characterized the feedback system, which stabilizes the sample position within one nanometer, and we have described the position control procedure, which enables movements of the sample while maintaining nanometer stability.

Such a stability can be maintained for very long periods of time (virtually without limits), allowing operation in high resolution microscopy, particle localization and tracking and single molecule experiments.

Moreover, the capability to manipulate the sample with a double optical tweezers setup can be utilized in nanomanipulation applications such as fabrication, positioning and fixation of nanostructures and single molecule experiments. A test performed on a single myosin motor interacting with an actin filament has demonstrated such capabilities in terms of stability and position control; in particular, the position of a single myosin molecule has been controlled with nanometer steps, showing that myosin binds in specific sites spaced about 5.6 nm along the actin filament.

A straightforward way of improving the feedback system would consist in improving the detection bandwidth. A bandwidth of the order of some kHz could be useful to drop off acoustic noise as well as thermal drifts and would enable investigating fast dynamic system with high precision. High bandwidths could be obtained either by using a CCD camera with a high frame rate, or by projecting the bead image on a quadrant detector photodiode, which could easily reach acquisition rates up to 10 kHz.

The authors thank R. Ballerini and A. Hajeb for their essential help in the development and construction of the mechanic structure of the microscope and M. Giuntini for the development of the QDP electronics. We also thank M. Canepari and R. Bottinelli (Dept. of Physiology, University of Pavia) for the biochemical preparations used in the acto-myosin experiments.

References

1. J.K. Gimzewski, C. Joachim, Science **283**, 1683 (1999)
2. D.G. Grier, Nature **424**, 810 (2003)
3. J. James, *Light microscopic techniques in biology and medicine* (The Netherlands, Amsterdam 1976), pp. 75
4. R.E. Thompson, D.R. Larson, W.W. Webb, Biophys. J. **82**, 2775 (2002)
5. R.N. Ghosh, W.W. Webb, Biophys. J. **66**, 1301 (1994)
6. U. Kubitscheck, O. Kuckmann, T. Kues, R. Peters, Biophys. J. **78**, 2170 (2000)
7. M. Goulian, S.M. Simon, Biophys. J. **79**, 2188 (2000)
8. L. Finzi, J. Gelles, Science **78**, 378 (1995)
9. W.H. Hell, Nature Biotechnology **21**, 1347 (2003)
10. A.D. Metha, M. Rief, J.A. Spudich, D.A. Smith, R.M. Simmons, Science **283**, 1689 (1999)
11. I.M. Toliç-Nørrelykke, L. Sacconi, G. Thon, F.S. Pavone, Current Biology **14**, 1181 (2004)
12. L. Sacconi, I.M. Toliç-Nørrelykke, R. Antolini, F.S. Pavone, J. Biomed. Opt. **10**, 014002 (2005)
13. P. Galajda, P. Ormos, Appl. Phys. Lett. **78**, 249 (2001)
14. J. Plewa, E. Tanner, D.M. Mueth, D. Grier, Optics Express **12**, 1978 (2004)
15. C. Mio, T. Gong, A. Terray, D.W.M. Marr, Fluid Phase Equilibria **185**, 157 (2001)
16. J. Won, T. Inaba, H. Masuhara, H. Fujiwara, K. Sasaki, S. Miawaki, S. Sato, Appl. Phys. Lett. **75**, 1506 (1999)
17. M.J. Lang, C.L. Asbury, J.W. Shaevitz, S.M. Block, Biophys. J. **83**, 491 (2002)
18. W. Steffen, D. Smith, R. Simmons, J. Sleep, PNAS **98**, 14949 (2001)
19. F. Gittes, C.F. Schmidt, Optics Lett. **23**, 7 (1998)
20. A.E. De Barr, *Automatic control. An introduction to the theory of feedback and feedback control system* (Chapman and Hall, London 1962)
21. J. Howard, *Mechanics of Motor Proteins and the Cytoskeleton* (Sinauer Associates, Inc. Publishers. Sunderland, Massachussetts, 2001)
22. J.T. Finer, R.M. Simmons, J.A. Spudich, Nature **368**, 113 (1994)
23. D.A. Smith, W. Steffen, R.M. Simmons, J. Sleep, Biophys. J. **81**, 2795 (2001)